

Geophysical Research Letters*



RESEARCH LETTER

10.1029/2023GL106125

Key Points:

- Newly homogenized radiosonde humidity and temperature data allow quantitative assessment of historical changes in atmospheric instability
- There are increasingly more unstable conditions with positive buoyancy in all seasons over most land areas from 1979 to 2020
- The increased unstable conditions mainly result from increased low-level moisture content and warmer air temperature

Supporting Information:

Supporting Information may be found in the online version of this article.

Correspondence to:

A. Dai and J. Chen, adai@albany.edu; chenjiaohope@163.com

Citation:

Chen, J., & Dai, A. (2023). The atmosphere has become increasingly unstable during 1979–2020 over the Northern Hemisphere. *Geophysical Research Letters*, *50*, e2023GL106125. https://doi.org/10.1029/2023GL106125

Received 28 AUG 2023 Accepted 7 OCT 2023

© 2023. The Authors.

This is an open access article under the terms of the Creative Commons Attribution-NonCommercial-NoDerivs License, which permits use and distribution in any medium, provided the original work is properly cited, the use is non-commercial and no modifications or adaptations are made.

The Atmosphere Has Become Increasingly Unstable During 1979–2020 Over the Northern Hemisphere

Jiao Chen¹ and Aiguo Dai²

¹Jiangsu Meteorological Observatory, Nanjing, China, ²Department of Atmospheric and Environmental Sciences, University at Albany, SUNY, Albany, NY, USA

Abstract Atmospheric instability affects the formation of convective storms, but how it has changed during recent decades is unknown. Here we analyze the occurrence frequency of stable and unstable atmospheric conditions over land using homogenized radiosonde data from 1979 to 2020. We show that atmospheric stable (unstable) conditions have decreased (increased) significantly by ~8%–32% (of time) from 1979 to 2020 over most land areas. In boreal summer, the mean positive buoyancy (i.e., convective available potential energy [CAPE]) also increases over East Asia while mean negative buoyancy (i.e., convective inhibition [CIN]) strengthens over Europe and North America from midnight-dawn for unstable cases. The increased unstable cases and mean CAPE result from increased low-level specific humidity and air temperature, which increase the buoyancy of a lifted parcel. The stronger CIN results from decreased near-surface relatively humidity and decreased lapse rate in the lower troposphere. Our results suggest that the atmosphere has become increasingly unstable, which could lead to more convective storms.

Plain Language Summary Severe weather events such as tornados and intense thunderstorms often cause significant loss of life and property. Their formation requires instability or unstable conditions in the atmosphere. Climate models project increased unstable conditions under greenhouse gas-induced global warming, but how atmospheric instability has changed during recent decades is unclear. Through analysis of newly homogenized radiosonde data, here we show that the atmosphere has become increasingly unstable over most land areas over the Northern Hemisphere from 1979 to 2020, with an increasing number of unstable conditions (i.e., with positive buoyancy) but a decreasing number of stable conditions (i.e., with zero or negative buoyancy). These changes result mainly from increased low-level moisture content and warmer air temperature. Such instability changes favor increased occurrence of convective storms.

1. Introduction

Atmospheric instability is necessary for the occurrence of convection (Seeley & Romps, 2015) and vertical mixing in the atmosphere. Thus, whether the atmosphere becomes increasingly unstable under greenhouse gas (GHG)-induced global warming has major implications for the occurrence of convective storms (Allen, 2018). Climate models project that both atmospheric convective available potential energy (CAPE), which is the positive buoyancy for a lifted parcel, and the convective inhibition (CIN), which is the negative buoyancy the parcel needs to overcome before reaching the level of free convection (LFC), would increase (Chen, Dai, Zhang, & Rasmussen, 2020; Rasmussen et al., 2020) while the stable conditions would decrease (Chen, Dai, Zhang, & Rasmussen, 2020) and severe unstable conditions would increase (Púčik et al., 2017; Rädler et al., 2019) over land under GHG-induced warming. The stronger CIN would allow the atmosphere to delay the onset of convection and thus accumulate more positive buoyancy before the onset of deep convection. This may contribute to the increase in heavy precipitation under GHG-induced warming (Dai et al., 2020; O'Gorman, 2015) and favor the formation of severe thunderstorms and hail (Allen et al., 2014; Diffenbaugh et al., 2013; Hoogewind et al., 2017). Thus, such a combination of CAPE and CIN changes would lead to a reduced number of atmospheric convection but increased intensity of deep convection (Del Genio et al., 2007), which is consistent with the overall decrease in precipitation frequency but large increases in heavy precipitation (Chen, Dai, & Zhang, 2020; Dai et al., 2020).

Over the recent years, violent storms and tornados have been observed frequently over the central-eastern United States (Gensini & Brooks, 2018; Kunkel et al., 2013; Tang et al., 2019) and other regions (Herring et al., 2022), often causing devastating damages and significant loss of human lives (Allen, 2018). The recent increases in severe storms are qualitatively consistent with the changes implied by the model-projected CAPE and CIN (Chen,

CHEN AND DAI 1 of 9

Dai, Zhang, & Rasmussen, 2020; Rasmussen et al., 2020) and other favorable environments for the formation of severe storms (Diffenbaugh et al., 2013; Glazer et al., 2021; Trapp et al., 2019). This raises important questions: How has the atmospheric thermodynamics changed during recent decades? Has the atmosphere become increasingly unstable and thus more favorable for the formation of convective storms over many land areas? Given the devastating damages currently occurring in the central-eastern United States and other regions (Gensini & Brooks, 2018; Herring et al., 2022) caused by violent storms, there is an urgent need for answers to these questions.

To examine recent changes in atmospheric conditions, one needs reliable long-term records of upper-air temperature and humidity. Radiosonde observations provide the only in-situ long-term data for atmospheric conditions; unfortunately, the raw radiosonde data for air temperature and humidity contain major discontinuities and spurious changes due to frequent changes in sounding sensors and observational practices (Dai et al., 2011; Haimberger et al., 2012; Zhou et al., 2021). Conventional data-quality controls by excluding problematic data points (e.g., Taszarek, Allen, Marchio, & Brooks, 2021) cannot remove spurious jumps in sounding records, and current reanalyses assimilate unhomogenized radiosonde humidity and other data, leading to similar spurious changes (Dai et al., 2011). As a result, unhomogenized sounding data and atmospheric reanalysis products, which show different trends for CAPE (Taszarek, Allen, Marchio, & Brooks, 2021), are not suitable for quantifying long-term changes in atmospheric conditions over China and other regions (Dai et al., 2011; Taszarek, Allen, Marchio, & Brooks, 2021). This results in a gap in our knowledge about historical changes in atmospheric instability, CAPE, CIN, and other atmospheric thermodynamic conditions, although there have been efforts to quantify changes in thermodynamics (Meukaleuni et al., 2016; Riemann-Campe et al., 2009) and storm environments (Li et al., 2020; Taszarek, Allen, Brooks, et al., 2021) using reanalysis data and quality-controlled radiosonde data (Pilguj et al., 2022; Taszarek, Allen, Marchio, & Brooks, 2021).

Here we analyze homogenized twice-daily radiosonde temperature and humidity data to examine the changes in the *occurrence frequency* of the atmospheric stable and unstable conditions over continents and many islands from 1979 to 2020 and the underlying causes. Two atmospheric thermodynamic conditions including CAPE = 0 cases (referred to as stable conditions) and CAPE > 0 cases (referred to as unstable conditions) are defined based on the skew-T log-P diagrams. Our results provide the first reliable assessment of atmospheric *instability* trends since 1979, which may have major implications for explaining recent changes in the occurrence frequency of severe storms and hail (Brooks et al., 2014; Gensini & Brooks, 2018; Herring et al., 2022; Tang et al., 2019). Our results also help validate findings based on unhomogenized radiosonde and reanalysis data from previous studies (e.g., Pilguj et al., 2022; Taszarek, Allen, Brooks, et al., 2021; Taszarek, Allen, Marchio, & Brooks, 2021) that often have a different focus from ours.

2. Data and Methods

2.1. Observational Data

We used the quality-controlled, homogenized twice-daily radiosonde humidity data of dewpoint depression (DPD) during 1958–2008 (Dai et al., 2011) and temperature (T) data during 1958–2020 (Zhou et al., 2021) at the surface and standard pressure levels. There are 991 matched stations that contain both homogenized DPD and T data from the two data sets. We also used the radiosonde DPD data from Integrated Global Radiosonde Archive version 2 (IGRA2), which was built from 33 different data sources with many quality controls but without temporal homogenization (Durre et al., 2018; referred to as the raw data). The last segment was used as the reference baseline and was not changed in the DPD homogenization (Dai et al., 2011). Given that discontinuities in most recent radiosonde records are small (Wang et al., 2013; Zhou et al., 2021), we simply used the IGRA2 humidity data after 2008 for the same 991 stations to extend the study period to 2020 by appending the IGRA2 DPD data from 2009 to 2020 to the homogenized DPD data from 1958 to 2008. Our analysis showed that this did not induce a discontinuity around 2008. Data series at 00:00 and 12:00 UTC (or 00Z and 12Z) were analyzed separately in this study. As shown by Dai et al. (2011) and Zhou et al. (2021), the homogenization removes major discontinuities in the sounding data and thus improves their homogeneity, which is important for trend analysis.

2.2. Methods

We calculated CAPE and CIN using the equations of Chen, Dai, Zhang, and Rasmussen (2020), assuming an air parcel is lifted from its original level (SFC) to LFC and then rises to the level of neutral buoyancy (EL). In this

CHEN AND DAI 2 of 9

study we only show the results for the reversible case. More details on data processing and calculations of CAPE and CIN are provided in Text S1 in Supporting Information S1.

There are two atmospheric conditions based on the CAPE and CIN values: (a) "CAPE = 0 cases," which include absolutely stable cases with CIN < 0 (continuous negative buoyancy from SFC to the stopping level) and neutral cases with CIN = 0 (well-mixed neutral conditions); (b) "CAPE > 0 cases," which include conditionally unstable cases with CIN < 0 (negative buoyancy from SFC to LFC and positive buoyancy from LFC to EL) and unstable cases with CIN = 0 (positive buoyancy starting from SFC to EL). Since a long-term change in the frequency of the CAPE = 0 cases may cause long-term mean changes in CAPE, it is better to examine the changes in the frequency of these two different conditions besides examining the mean CAPE and CIN changes.

To balance sampling homogeneity and minimizing data gaps, we require at least 30 days with valid soundings and at least 5 days with valid soundings for two of the 3 months in order to have a valid seasonal mean. Climatology and trend calculations are based on 1979–2020 to facilitate comparisons with reanalysis data, which often start in 1979. This is also because sounding data before 1979 are less reliable and sparser. We only included stations with at less 20 years of valid data during 1979–2020 in our analysis. We averaged the station anomalies to derive a regional-mean time series requiring each year to have at least as many stations as half of the long-term mean. Our focus is on the long-term change. Tests showed that using non-parametric methods yielded similar trend patterns as revealed by the least squares estimate shown below.

3. Results

3.1. Increasing Occurrence of Atmospheric Unstable Conditions

We find that atmospheric unstable conditions (i.e., CAPE > 0 cases) have increased significantly by 2%-8% of time per decade (i.e., an increase in absolute frequency), which amounts to a cumulative increase of \sim 8%-32% (of time) from 1979 to 2020, over most land areas in both boreal winter (December-January-February or DJF) and summer (June-July-August or JJA), especially over Europe, East Asia (EA) and North America (NA) where observations are relatively dense and reliable, while the stable conditions (i.e., CAPE = 0 cases) have decreased by similar amounts over these regions (Figure 1). Such a change rate is very rapid and alarming compared to those for other atmospheric fields (e.g., water vapor, Wang et al., 2016). Time series of the unstable occurrence frequency averaged over EA, NA, and Europe (EU) all show significant and often fast increases in all seasons, especially over EU and NA (Figure S2 in Supporting Information S1). For example, summer frequency of the unstable conditions increased from \sim 54%, 56%, and 50% (of time) in 1979 to \sim 72%, 71%, and 63% in 2020 over EA, NA, and EU, respectively. These changes represent a percentage increase of 26%-33%. Although we mainly show the results in JJA and DJF, the increasing (decreasing) trends for the unstable (stable) conditions are consistent among different seasons.

The CAPE and CIN values are determined by atmospheric humidity and temperature profiles, which are illustrated on the skew-T log-P diagram (Figure S1a in Supporting Information S1). The specific humidity (q) and T at the lifting level determine the parcel path and its lapse rates. The lifted air parcel will first rise following the dry adiabat up to the lifting condensation level (LCL), above which the ascending parcel will follow a moist adiabat. Higher q and T of the lifted parcel would result in more latent heating and thus slower cooling with height above the LCL, which shifts the parcel path toward to the right-hand side and thus increases the chance for it to intersect with atmospheric temperature profile on the skew-T log-P diagram (Figure S1b in Supporting Information S1), resulting in more cases with positive buoyancy.

Indeed, over EA and EU in both DJF and JJA, increased near-surface q and T are associated with increased occurrence of unstable cases, with positive correlations with the frequency of the CAPE > 0 cases, especially in JJA (Figures 2a, 2b, 2e, and 2f). Over NA, the increased RH besides higher q (Figures 2c and 2d) would lead to decreased LCL (Chen, Dai, Zhang, & Rasmussen, 2020) and thus earlier start of the moist adiabat, which would also contribute to more CAPE > 0 cases. The RH over EA also increased and partly contributed to the increased frequency of the CAPE > 0 cases there (Figures 2a and 2b), while the RH over EU generally decreased, which would increase LCL, and showed negative correlations with the frequency of the unstable cases, especially at 12Z (Figures 2e and 2f). The changes in near-surface T over NA do not show obvious relationships with the frequency changes of the unstable conditions (Figures 2c and 2d). Thus, the increased unstable cases resulted mainly from increased low-level q and T (except for NA where T's role is small), with some contributions also from increased RH over NA and EA.

CHEN AND DAI 3 of 9

onlinelibrary.wiley.com/doi/10.1029/2023GL106125 by Suny University At Albany, Wiley Online Library on [23/10/2023]. See

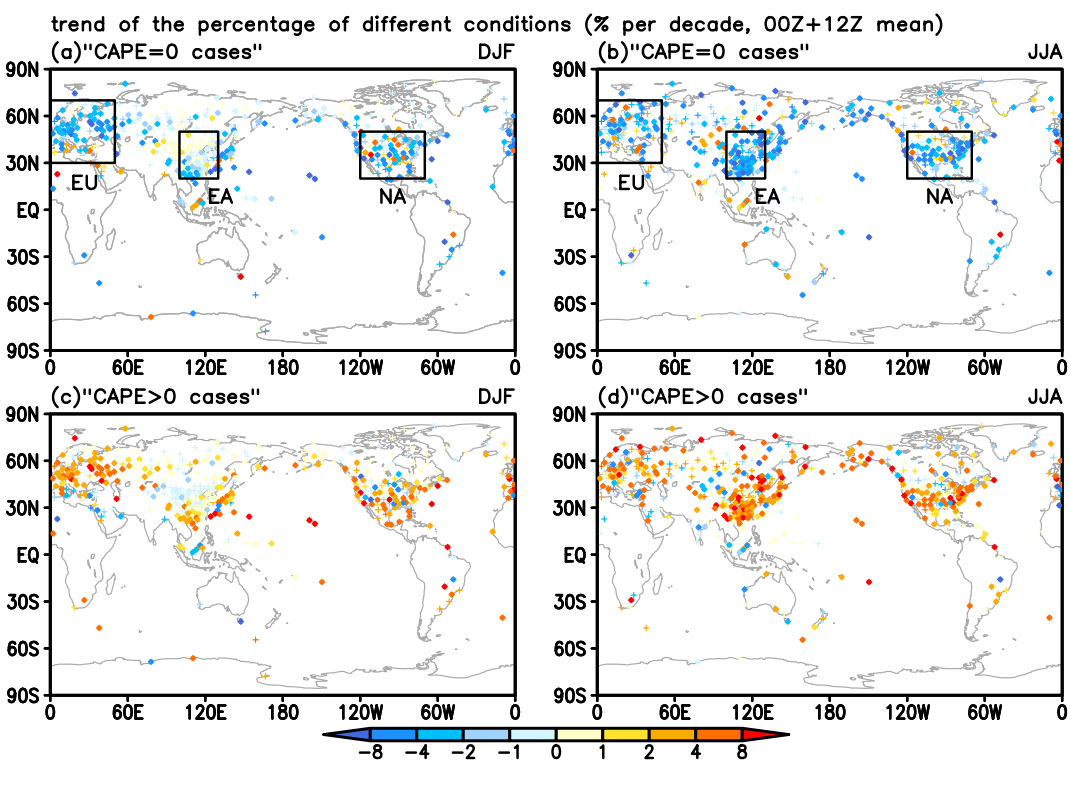


Figure 1. Changes in the occurrence frequency of stable and unstable cases. Distributions of the linear trend (in % of all valid reports per decade, averaged over the 00 and 12Z observation times) of the occurrence frequency of (a, b) "CAPE = 0 cases" (stable) and (c, d) "CAPE > 0 cases" (unstable) during 1979–2020 in (left) DJF and (right) JJA at individual stations. Filled diamonds (colored crosses) indicate statistically significant (insignificant) trends at the 95% confidence level based on a two-tailed Student's t test. East Asia (100°–130°E, 20°–50°N), North America (120°–70°W, 20°–50°N), and EU (0°–50°E, 30°–70°N) outlined in panels (a, b) are selected regions for calculating regional mean time series.

3.2. Increased Mean CAPE During Daytime and Enhanced Mean CIN From Midnight-Dawn

Fewer stable cases would lead to an increase in the overall mean CAPE. Thus, we should not only examine the CAPE trend averaged over all valid reports (Figures 3e and 3f), but also decompose the CAPE trend into two terms (see Text S2 in Supporting Information S1): (a) term1 due to the trend in the occurrence frequency of CAPE > 0 cases (Figures 3a and 3b) and (b) term2 due to the trend in the mean CAPE values averaged over all the CAPE > 0 cases (Figures 3c and 3d). Mean CAPE averaged over all valid reports in JJA has significantly increased mainly over EA at both 00Z and 12Z, and over parts of southern NA at 00Z or Europe at 12Z (Figures 3e and 3f), which is similar to the distributions of the mean CAPE changes from term2 (Figures 3c and 3d). In other words, mean CAPE increases mainly during daytime (around 90° E- 60° W at 00Z and 0° - 140° E at 12Z; the corresponding local time is 06:00-20:00 and 12:00-21:00), when the atmosphere is most unstable. The increased occurrence frequency of the CAPE > 0 cases result in increased mean CAPE over most land areas (Figures 3a and 3b) as expected, but with relatively small amplitudes. As a result, the mean CAPE change averaged over all conditions is dominated by the mean CAPE change for the CAPE > 0 cases, which show increased CAPE mainly during daytime when convection typically occurs over most land areas (Dai et al., 2007).

Because the stable cases often correspond to large negative buoyancy that would dominate the overall CIN change if they were included in the averaging, we should quantify the changes of the negative buoyancy for the CAPE = 0 and CAPE > 0 cases separately (Figure 4). For the stable cases, we find that the JJA mean CIN has weakened over Europe and EA at 00Z and over EA and central NA at 12Z, which indicates that the stable conditions are becoming less stable from night-early morning (around 0° - 140° E at 00Z and 90° E- 60° W at 12Z; the corresponding local time is 00:00-09:00 and 18:00-08:00) besides its frequency decreases. For the unstable cases, the mean CIN has strengthened mainly over Europe at 00Z and over NA at 12Z, which indicates that CIN's strengthening occurred mainly from midnight-dawn (around 0° - 60° E at 00Z and 120° - 90° W at 12Z; the corresponding local time is 00:00-04:00 and 04:00-06:00). Moreover, the mean CIN has weakened over EA at

CHEN AND DAI 4 of 9

19448007, 2023, 20, Downloaded from https://agupubs.onlinelibrary.wiley.com/doi/10.1029/2023GL106125 by Suny University At Albany, Wiley Online Library on [23/10/2023]. See the Terms and Conditions (https://agupubs.onlinelibrary.wiley.com/doi/10.1029/2023GL106125 by Suny University At Albany, Wiley Online Library on [23/10/2023]. See the Terms and Conditions (https://agupubs.onlinelibrary.wiley.com/doi/10.1029/2023GL106125 by Suny University At Albany, Wiley Online Library on [23/10/2023]. See the Terms and Conditions (https://agupubs.onlinelibrary.wiley.com/doi/10.1029/2023GL106125 by Suny University At Albany, Wiley Online Library on [23/10/2023]. See the Terms and Conditions (https://agupubs.onlinelibrary.wiley.com/doi/10.1029/2023GL106125 by Suny University At Albany, Wiley Online Library on [23/10/2023]. See the Terms and Conditions (https://agupubs.onlinelibrary.wiley.com/doi/10.1029/2023GL106125 by Suny University At Albany, Wiley Online Library on [23/10/2023]. See the Terms and Conditions (https://agupubs.onlinelibrary.wiley.com/doi/10.1029/2023GL106125 by Suny University At Albany, Wiley Online Library on [23/10/2023]. See the Terms and Conditions (https://agupubs.onlinelibrary.wiley.com/doi/10.1029/2023GL106125 by Suny University At Albany, Wiley Online Library on [23/10/2023]. See the Terms and Conditions (https://agupubs.onlinelibrary.wiley.com/doi/10.1029/2023GL106125 by Suny University At Albany, Wiley Online Library on [23/10/2023]. See the Terms and Conditions (https://agupubs.onlinelibrary.wiley.com/doi/10.1029/2023GL106125 by Suny University At Albany, Wiley Online Library on [23/10/2023]. See the Terms and Conditions (https://agupubs.onlinelibrary.wiley.com/doi/10.1029/2023GL106125 by Suny University At Albany, Wiley Online Library on [23/10/2023]. See the Terms and Conditions (https://agupubs.onlinelibrary.wiley.com/doi/10.1029/2023GL106125 by Suny University At Albany, Wiley Online Library on [23/10/2023]. See the Terms and Conditions (https://agupubs.onlinelibrary.wiley.com/doi/10.1029/20

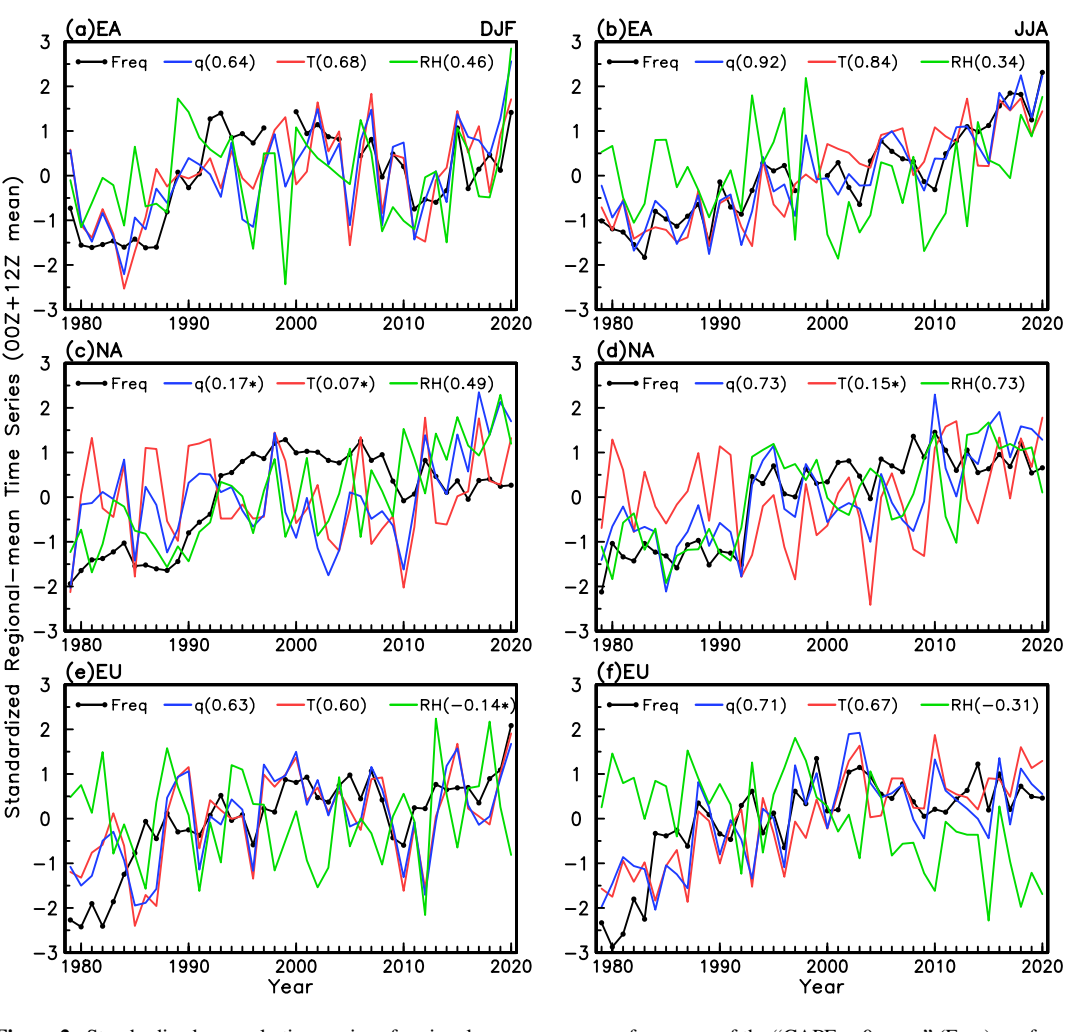


Figure 2. Standardized anomaly time series of regional mean occurrence frequency of the "CAPE > 0 cases" (Freq), surface q, surface T and surface RH in (left) DJF and (right) JJA averaged over the 00 and 12Z observation times for regions outlined in Figures 1a and 1b. The correlation coefficients between Freq and q or T or RH are given in the parentheses (which are significant at the 95% confidence level except for the values marked by *).

both 00Z and 12Z, southern NA at 00Z and Europe at 12Z with increased CAPE there, which favors convection during daytime.

We further examine the changes in the histograms of CAPE and CIN from 1979–1999 to 2000–2020 (Figure S3 in Supporting Information S1) to reveal the occurrence frequency changes of CAPE and CIN as a function of their mean magnitudes. There are large increases in the cases with small positive CAPE (i.e., 0–100 J kg $^{-1}$) at both 00Z and 12Z over NA and EU, where the changes in the cases with large CAPE (i.e., 100–2,500 J kg $^{-1}$) are small. In other words, some CAPE = 0 cases are likely to become new CAPE > 0 cases with relatively small positive values in the later years; including these small-CAPE cases in the averaging would bring down the mean CAPE values for the later years, resulting in downward CAPE trends when averaged over only the CAPE > 0 cases at many NA and EU stations (Figures 3c and 3d). Over EA, however, the increase of the cases with low CAPE is small while there are large increases of the cases with large CAPE. This results in increased mean CAPE averaged over all CAPE > 0 cases over EA at both 00Z and 12Z. More specifically, for the CAPE trends averaged over all reports over NA and EU (Figures 3e and 3f), the small changes of the cases with large CAPE dominate over the positive contributions from the increased frequency of small CAPE cases (Figure S4 in Supporting Information S1), resulting in small or negative CAPE trends over these regions.

For CIN changes (right panels of Figure S3 in Supporting Information S1), there are fewer small-CIN cases (i.e., -1 to -20 J kg $^{-1}$) and more large-CIN cases (i.e., stronger than -20 J kg $^{-1}$) over NA at 12Z and over EU at 00Z

CHEN AND DAI 5 of 9

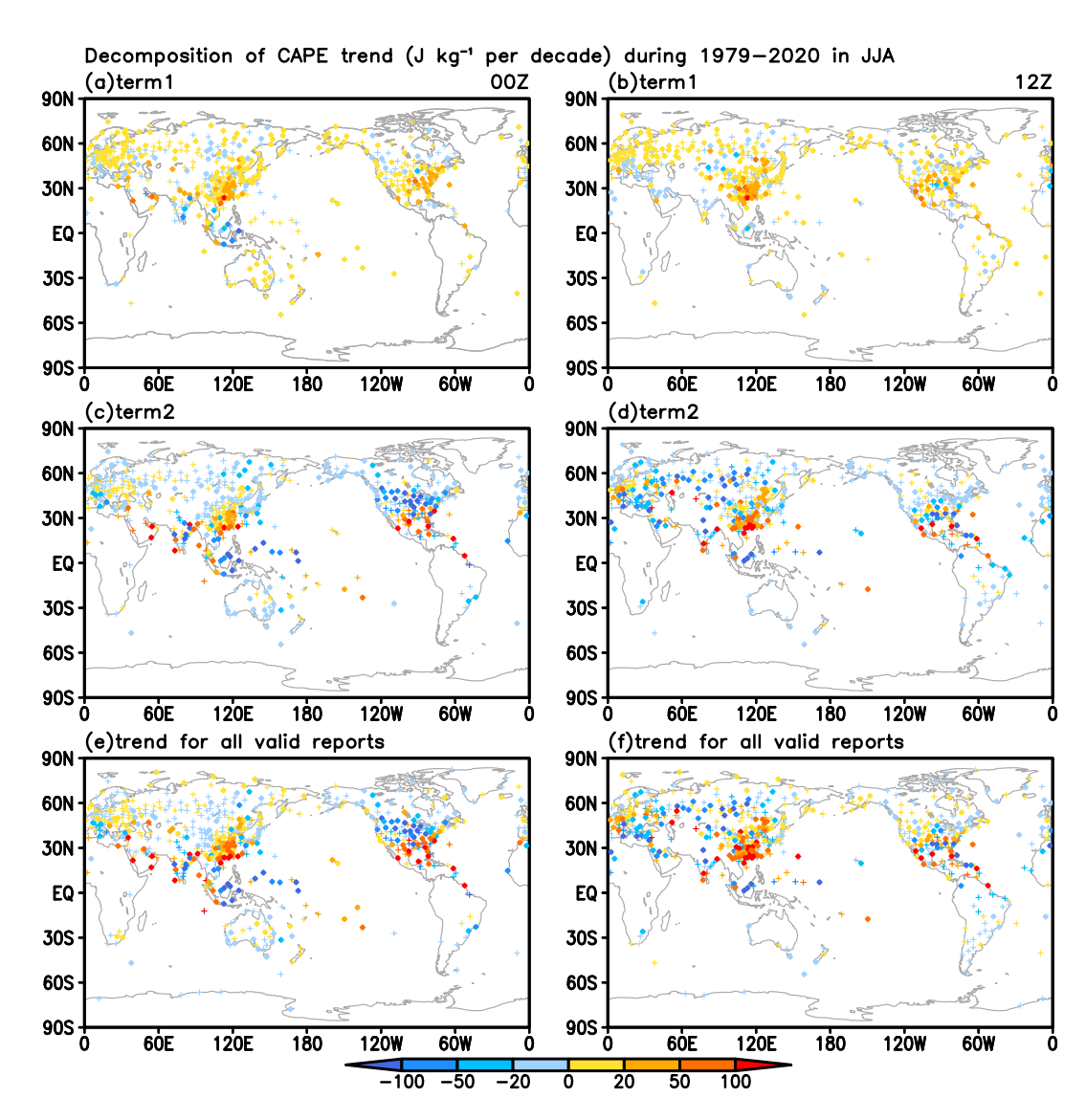


Figure 3. Changes in JJA mean convective available potential energy (CAPE) under different conditions. The two components of the linear trend of mean CAPE for all valid reports due to (a, b) changes in the occurrence frequency of "CAPE > 0 cases" (term1) and (c, d) changes in the mean CAPE values of "CAPE > 0 cases" (term2), and (e, f) the real linear trend of mean CAPE for all valid reports in JJA during 1979–2020 at (left) 00Z and (right) 12Z, respectively. Filled diamonds (colored crosses) indicate statistically significant (insignificant) trends at the 95% confidence level based on a two-tailed Student's *t* test.

in JJA, which results in enhanced mean CIN there (Figures 4b and 4d). There are also fewer small-CIN cases (i.e., -3 to -20 J kg $^{-1}$) and more large-CIN cases over EA at both 00Z and 12Z, but the very small-CIN cases (i.e., 0 to -3 J kg $^{-1}$) increased a lot, which greatly weakens the mean CIN there (Figures 4b and 4d). The large-CIN cases decreased together with increased very small-CIN cases over NA at 00Z, while over EU at 12Z the increases in large-CIN cases are smaller than the decreases in small-CIN cases, together with increased very small-CIN cases, both contributing to the weakened mean CIN there (Figures 4b and 4d).

The changes in the path of the lifted air parcel and atmospheric temperature profiles both influence the CAPE and CIN values. The time series and corresponding correlation coefficients (Figure S5 in Supporting Information S1) suggest that the increased EL or decreased LFC contributes to increased CAPE over EA at both 00Z and 12Z, which results from the increased low-level q through increased latent heating above LFC. The increased LCL and LFC contribute to the enhanced CIN over EU at 00Z and over NA at 12Z, which results from the decreased low-level RH. At the same time, the decreased low-level lapse rates indicate a shift of the low-level environmental

CHEN AND DAI 6 of 9

from https://agupubs.onlinelibrary.wiley.com/doi/10.1029/2023GL106125 by Suny University At Albany, Wiley Online Library on [23/10/2023]. See the Terms

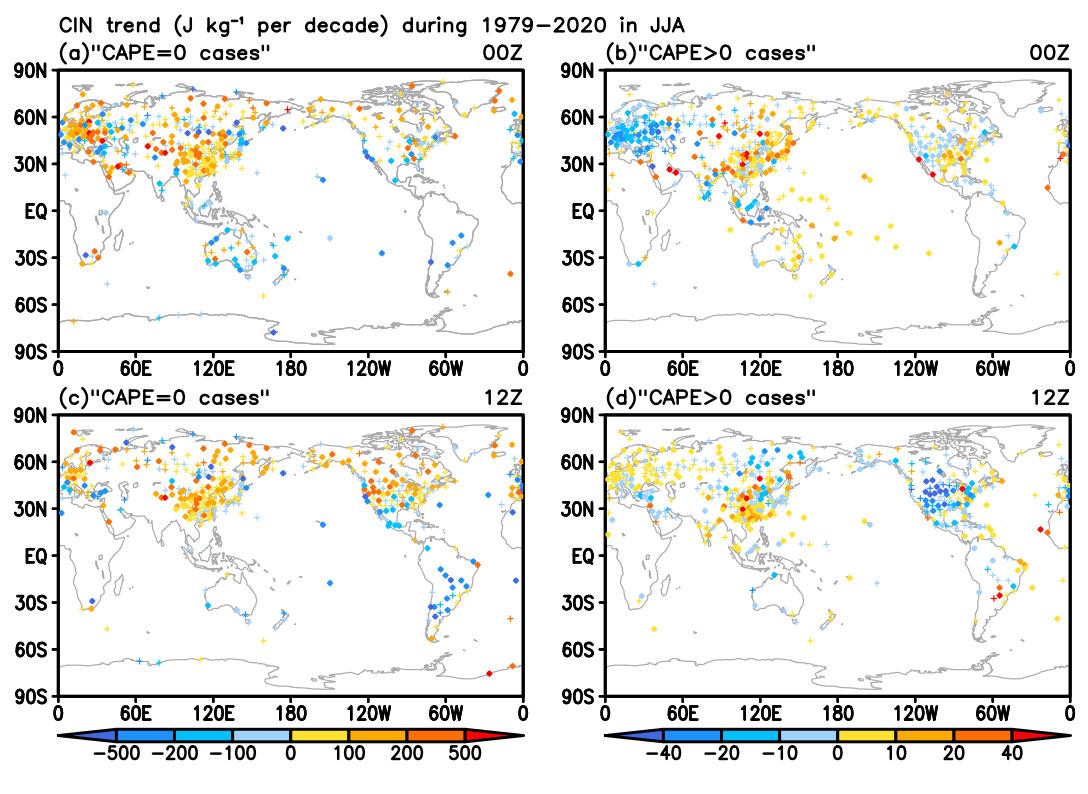


Figure 4. Distributions of the linear trend of JJA mean convective inhibition (CIN) for (left) "CAPE = 0 cases" and (right) "CAPE > 0 cases" during 1979–2020 at (a, b) 00Z and (c, d) 12Z, respectively. Filled diamonds (colored crosses) indicate statistically significant (insignificant) trends at the 95% confidence level based on a two-tailed Student's *t* test. A positive (negative) trend indicates that the negative CIN becomes less negative or weakening (more negative or strengthening).

temperature profile toward to the right-hand side on the skew-T log-P diagram, also contributing to more negative buoyancy during 1979–2020. Over NA (Figure S6 in Supporting Information S1), the decreased mid to low-level lapse rates at both 00Z and 12Z indicates a shift of the environmental temperature profile on the mid-low levels toward to the right-hand side on the skew-T log-P diagram, thus contributing to lower EL and less positive buoyancy. The decreased q at 12Z also partly contributes to the decreased CAPE there.

4. Summary and Discussion

In this study we analyzed newly homogenized radiosonde data to examine historical changes from 1979 to 2020 in the occurrence frequency of atmospheric stable and unstable conditions defined using CAPE and CIN, rather changes in the CAPE and CIN values as in previous studies. We found that the unstable (i.e., CAPE > 0) conditions have become more frequent and increased by ~8%-32% (of time) from 1979 to 2020 over most land areas mainly in the Northern Hemisphere, while the stable conditions (i.e., CAPE = 0) decreased by similar amounts. Over NA, Europe and EA, summer unstable cases have increased by a quarter to one third from 1979 to 2020. Such a rapid increase in atmospheric unstable conditions results from increased low-level q and T (except for NA), which lead to a shift of the parcel path toward to the right-hand side on the skew-T log-P diagrams, with some additional contributions from increased low-level RH over NA and EA. In JJA, the mean CAPE increases significantly over EA while mean CIN mainly strengthens over Europe and NA from midnight-dawn for CAPE > 0 cases. The stronger CIN over Europe at 00Z and over central NA at 12Z result from the decreased near-surface RH and decreased lapse rate in the lower troposphere, which lead to a higher LCL and LFC for the CAPE > 0 cases. The results suggest that the atmosphere over most land areas mainly in the Northern Hemisphere has become increasingly unstable as near-surface q and T increase, which favors the formation of convective storms. Although the stations mainly cover Northern Hemisphere land, the consistency of the trends at the sparsely distributed stations in the tropics and Southern Hemisphere (Figure 1) seems to suggest that the global atmosphere has become increasingly unstable.

CHEN AND DAI 7 of 9

19448007, 2023, 20, Downloa

Chen, Dai, Zhang, and Rasmussen (2020) showed that under GHG-induced global warming, future stable cases would decrease over land areas, which implies increased unstable cases. Púčik et al. (2017) and Rädler et al. (2019) reported increased occurrence of unstable environments in central-southern Europe by the late 21st century. The historical changes in the stable (unstable) cases reported here are qualitatively consistent with the model-projected future changes. Chen, Dai, Zhang, and Rasmussen (2020) also reported that there is a shift of the low-CAPE and weak-CIN cases toward high-CAPE and strong-CIN cases. For the historical changes (Figure S3 in Supporting Information S1), we see a similar behavior only for the CIN changes except for NA at 00Z. For the CAPE changes, we only see large increases in large-CAPE cases over EA where low-CAPE cases did not decrease. The CIN changes presented here are qualitatively consistent with previous studies using ERA5 reanalysis or quality-controlled rawinsonde data (Pilguj et al., 2022; Taszarek, Allen, Brooks, et al., 2021), which showed robust stronger CIN over most of the United States and modest CIN increases over Europe during recent decades. The decreased CAPE over EA in ERA5 which used unhomogenized radiosonde data (except for temperature), differs from the robust CAPE increase using quality-controlled but unhomogenized rawinsonde observations (Taszarek, Allen, Marchio, & Brooks, 2021) or homogenized radiosonde data here. Moreover, the mixed trends of the 95th percentile of CAPE over Europe and NA in Taszarek, Allen, Marchio, and Brooks (2021) also partly differ from our results. These comparisons indicate that homogenization may qualitatively impact the small trends of CAPE over Europe and NA while only has a quantitative impact on the strong trends in CIN over NA and CAPE over EA. Thus, improvements in the homogeneity in both radiosonde and reanalysis data are needed. Using homogenized radiosonde data in both atmospheric reanalyses and long-term change studies would be a step forward. Finally, the historical changes examined here contain not only GHG-induced long-term changes, but also other changes due to recent anthropogenic and natural aerosol changes, and decadal oscillations due to internal variability (Qin et al., 2020). Thus, some inconsistency with the model-projected changes should be expected.

Data Availability Statement

The IGRA2 radiosonde data are available at NOAA National Centers for Environmental Information via Durre et al. (2016). The homogenized radiosonde data are available at Mendeley Data via https://doi.org/10.17632/8r4z4wvyp4.1.

References

Allen, J. T. (2018). Climate change and severe thunderstorms. In Oxford research encyclopedia of climate science. https://doi.org/10.1093/acrefore/9780190228620.013.62

Allen, J. T., Karoly, D. J., & Walsh, K. J. (2014). Future Australian severe thunderstorm environments. Part II: The influence of a strongly warming climate on convective environments. *Journal of Climate*, 27(10), 3848–3868. https://doi.org/10.1175/JCLI-D-13-00426.1

Brooks, H. E., Carbin, G. W., & Marsh, P. T. (2014). Increased variability of tornado occurrence in the United States. *Science*, 346(6207), 349–352. https://doi.org/10.1126/science.1257460

Chen, J., Dai, A., & Zhang, Y. (2020). Linkage between projected precipitation and atmospheric thermodynamic changes. *Journal of Climate*, 33(16), 7155–7178. https://doi.org/10.1175/JCLI-D-19-0785.1

Chen, J., Dai, A., Zhang, Y., & Rasmussen, K. L. (2020). Changes in convective available potential energy and convective inhibition under global warming. *Journal of Climate*, 33(6), 2025–2050. https://doi.org/10.1175/JCLI-D-19-0461.1

Dai, A., Lin, X., & Hsu, K.-L. (2007). The frequency, intensity, and diurnal cycle of precipitation in surface and satellite observations over low-and mid-latitudes. Climate Dynamics, 29(7–8), 727–744. https://doi.org/10.1007/s00382-007-0260-y

Dai, A., Rasmussen, R. M., Liu, C., Ikeda, K., & Prein, A. F. (2020). A new mechanism for warm-season precipitation response to global warming based on convection-permitting simulations. *Climate Dynamics*, 55(1–2), 343–368. https://doi.org/10.1007/s00382-017-3787-6

Dai, A., Wang, J., Thorne, P. W., Parker, D. E., Haimberger, L., & Wang, X. L. (2011). A new approach to homogenize daily radiosonde humidity data. *Journal of Climate*, 24(4), 965–991. https://doi.org/10.1175/2010JCLI3816.1

Del Genio, A. D., Yao, M.-S., & Jonas, J. (2007). Will moist convection be stronger in a warmer climate? *Geophysical Research Letters*, 34(16), L16703. https://doi.org/10.1029/2007GL030525

Diffenbaugh, N. S., Scherer, M., & Trapp, R. J. (2013). Robust increases in severe thunderstorm environments in response to green-house forcing. *Proceedings of the National Academy of Sciences of the United States of America*, 110(41), 16361–16366. https://doi.org/10.1073/pngs.1307758110

Durre, I., Yin, X., Vose, R. S., Applequist, S., & Arnfield, J. (2018). Enhancing the data coverage in the integrated global radiosonde archive. Journal of Atmospheric and Oceanic Technology, 35(9), 1753–1770. https://doi.org/10.1175/JTECH-D-17-0223.1

Durre, I., Yin, X., Vose, R. S., Applequist, S., Arnfield, J., Korzeniewski, B., & Hundermark, B. (2016). Integrated global radiosonde archive (IGRA) version 2 [Dataset]. NOAA National Centers for Environmental Information. https://doi.org/10.7289/V5X63K0Q

Gensini, V. A., & Brooks, H. E. (2018). Spatial trends in United States tornado frequency. NPJ Climate and Atmospheric Science, 1(1), 38. https://doi.org/10.1038/s41612-018-0048-2

Glazer, R. H., Torres-Alavez, J. A., Coppola, E., Giorgi, F., Das, S., Ashfaq, M., & Sines, T. (2021). Projected changes to severe thunderstorm environments as a result of twenty-first century warming from RegCM CORDEX-CORE simulations. Climate Dynamics, 57(5–6), 1595– 1613. https://doi.org/10.1007/s00382-020-05439-4

Acknowledgments

Chen was supported by the National Natural Science Foundation of China (Grant 42105038). Dai acknowledges the support by the U.S. National Science Foundation (Grants AGS-2015780 and OISE-1743738).

CHEN AND DAI 8 of 9

- Haimberger, L., Tavolato, C., & Sperka, S. (2012). Homogenization of the global radiosonde temperature dataset through combined comparison with reanalysis background series and neighboring stations. *Journal of Climate*, 25(23), 8108–8131. https://doi.org/10.1175/JCLI-D-11-00668.1
 Herring, S. C., Christidis, N., Hoell, A., & Stott, P. A. (Eds.) (2022). *Explaining extreme events of 2020 from a climate perspective* (Vol. 103, No.
- (3)). Bulletin of the American Meteorological Society. https://doi.org/10.1175/BAMS-ExplainingExtremeEvents2020.1
- Hoogewind, K. A., Baldwin, M. E., & Trapp, R. J. (2017). The impact of climate change on hazardous convective weather in the United States: Insight from high-resolution dynamical downscaling. *Journal of Climate*, 30(24), 10081–10100. https://doi.org/10.1175/JCLI-D-16-0885.1
- Kunkel, K. E., Karl, T. R., Brooks, H., Kossin, J., Lawrimore, J. H., Arndt, D., et al. (2013). Monitoring and understanding trends in extreme storms: State of knowledge. Bulletin of the American Meteorological Society, 94(4), 499–514. https://doi.org/10.1175/BAMS-D-11-00262.1
- Li, F., Chavas, D. R., Reed, K. A., & Dawson, D. T., II. (2020). Climatology of severe local storm environments and synoptic-scale features over North America in ERA5 reanalysis and CAM6 simulation. *Journal of Climate*, 33(19), 8339–8365. https://doi.org/10.1175/JCLI-D-19-0986.1
- Meukaleuni, C., Lenouo, A., & Monkam, D. (2016). Climatology of convective available potential energy (CAPE) in ERA-Interim reanalysis over West Africa. *Atmospheric Science Letters*, 17(1), 65–70. https://doi.org/10.1002/asl.601
- O'Gorman, P. (2015). Precipitation extremes under climate change. Current Climate Change Reports, 1(2), 49–59. https://doi.org/10.1007/s40641-015-0009-3
- Pilguj, N., Taszarek, M., Allen, J. T., & Hoogewind, K. A. (2022). Are trends in convective parameters over the United States and Europe consistent between reanalyses and observations? *Journal of Climate*, 35(12), 3605–3626. https://doi.org/10.1175/JCLI-D-21-0135.1
- Púčik, T., Groenemeijer, P., Rädler, A. T., Tijssen, L., Nikulin, G., Prein, A. F., et al. (2017). Future changes in European severe convection environments in a regional climate model ensemble. *Journal of Climate*, 30(17), 6771–6794. https://doi.org/10.1175/JCLI-D-16-0777.1
- Qin, M., Dai, A., & Hua, W. (2020). Aerosol-forced multidecadal variations across all ocean basins in models and observations since 1920. Science Advances, 6(29), eabb0425. https://doi.org/10.1126/sciadv.abb0425
- Rädler, A. T., Groenemeijer, P. H., Faust, E., Sausen, R., & Púčik, T. (2019). Frequency of severe thunderstorms across Europe expected to increase in the 21st century due to rising instability. npj Climate and Atmospheric Science, 2(1), 30. https://doi.org/10.1038/s41612-019-0083-7
- Rasmussen, K. L., Prein, A. F., Rasmussen, R. M., Ikeda, K., & Liu, C. (2020). Changes in the convective population and thermodynamic environments in convection-permitting regional climate simulations over the United States. *Climate Dynamics*, 55(1–2), 383–408. https://doi. org/10.1007/s00382-017-4000-7
- Riemann-Campe, K., Fraedrich, K., & Lunkeit, F. (2009). Global climatology of convective available potential energy (CAPE) and convective inhibition (CIN) in ERA-40 reanalysis. *Atmospheric Research*, 93(1–3), 534–545. https://doi.org/10.1016/j.atmosres.2008.09.037
- Seeley, J. T., & Romps, D. M. (2015). The effect of global warming on severe thunderstorms in the United States. *Journal of Climate*, 28(6), 2443–2458. https://doi.org/10.1175/JCLI-D-14-00382.1
- Tang, B. H., Gensini, V. A., & Homeyer, C. R. (2019). Trends in United States large hail environments and observations. NPJ Climate and Atmospheric Science, 2(1), 45. https://doi.org/10.1038/s41612-019-0103-7
- Taszarek, M., Allen, J. T., Brooks, H. E., Pilguj, N., & Czernecki, B. (2021). Differing trends in United States and European severe thunder-storm environments in a warming climate. Bulletin of the American Meteorological Society, 102(2), E296–E322. https://doi.org/10.1175/BAMS-D-20-0004.1
- Taszarek, M., Allen, J. T., Marchio, M., & Brooks, H. E. (2021). Global climatology and trends in convective environments from ERA5 and rawinsonde data. NPJ Climate and Atmospheric Science, 4(1), 35. https://doi.org/10.1038/s41612-021-00190-x
- Trapp, R. J., Hoogewind, K. A., & Lasher-Trapp, S. (2019). Future changes in hail occurrence in the United States determined through convection-permitting dynamical downscaling. *Journal of Climate*, 32(17), 5493–5509. https://doi.org/10.1175/JCLI-D-18-0740.1
- Wang, J., Dai, A., & Mears, C. (2016). Global water vapor trend from 1988 to 2011 and its diurnal asymmetry based on GPS, radiosonde, and microwave satellite measurements. *Journal of Climate*, 29(14), 5205–5222. https://doi.org/10.1175/JCLI-D-15-0485.1
- Wang, J., Zhang, L., Dai, A., Immler, F., Sommer, M., & Vömel, H. (2013). Radiation dry bias correction of Vaisala RS92 humidity data and its impacts on historical radiosonde data. *Journal of Atmospheric and Oceanic Technology*, 30(2), 197–214. https://doi.org/10.1175/
- Zhou, C., Wang, J., Dai, A., & Thorne, P. W. (2021). A new approach to homogenize global subdaily radiosonde temperature data from 1958 to 2018. *Journal of Climate*, 34(3), 1163–1183. https://doi.org/10.1175/JCLI-D-20-0352.1

CHEN AND DAI 9 of 9